DOI 10.5162/sensor2015/B8.3

Using a high speed camera for high resolution 3D measurements of sound-flow interaction

André Döring[1], Johannes Gürtler[1], Daniel Haufe[1], Anita Schulz[3], Friedrich Bake[3], Lars Enghardt[2,3], Jürgen Czarske[1], Andreas Fischer[1]
[1] Laboratory of Measurement and Testing Techniques, Department of Electrical Engineering and Information Technology, TU Dresden, Helmholtzstr. 18, 01069 Dresden, Germany
E-Mail: andreas.fischer2@tu-dresden.de
[2] Institute of Fluid Dynamics and Technical Acoustics, TU Berlin, 10623 Berlin, Germany
[3] Institute of Propulsion Technology, German Aerospace Center (DLR), 10623 Berlin, Germany

Abstract
We present a novel approach of using a high-speed camera to combine a frequency modulated Doppler global velocimetry (FM-DGV) system and a particle image velocimetry (PIV) system in order to monitor the 3D velocity field with an increased spatial resolution of $300\ \mu\mathrm{m}$. This approach facilitates a simultaneous measurement of all three velocity components with a high measurement rate of $10\ \mathrm{kHz}$. Hence, the sound induced oscillation velocities for tone frequencies of several kHz can be resolved in addition to the mean flow velocity. Therefore, the measurement system is promising for investigating the sound-flow interaction, which is demonstrated for the analysis of the sound damping mechanism at a bias flow liner used for aircraft noise reduction.

Key words: flow measurement, acoustic damping, bias flow liner, FM-DGV, PIV

1. Introduction

The optimization of bias flow liners, i.e. perforated walls with a cavity behind, in combustion chambers promises a significant reduction of aircraft noise. Here, a better understanding of the occurring damping phenomena is indispensable for a maximization of the damping performance. This makes it mandatory to examine the interaction of the acoustic velocity with the flow velocity [1]. Due to the disparity of the temporal and spatial scales of the sound and flow field, current simulation techniques are unable to give a sufficient explanation with reasonable effort. Hence, measurement techniques are needed that allow a non-intrusive acquisition of the fluid velocity field with a high temporal and spatial resolution. The frequency modulated Doppler global velocimetry (FM-DGV) is able to measure both, the acoustically induced particle oscillation and the flow velocity, simultaneously [2]. However, the FM-DGV system used in [2] and [3] has three considerable disadvantages: (i) the system has a limited spatial resolution of about $800\ \mu\mathrm{m}$, (ii) due to the usage of a linear detector array a high traversing effort is inevitable to cover a 3D region of interest and (iii) only one velocity component is detected at once. In order to overcome these drawbacks, the applicability of a Phantom v1610 high-speed camera in combination with a FM-DGV system is investigated. The spatial resolution of the FM-DGV system using a high-speed camera is in principle only limited by the sensor pixel size. It is successfully demonstrated that spatial resolution can be improved at least to 220 x220 µm². Moreover, the planar measurement reduces the traversing effort significantly. To measure the entire planar flow velocity field simultaneously with a single camera the applicability of PIV evaluation algorithms on the FM-DGV data is demonstrated. Here, FM-DGV provides the out-of-plane velocity component, while PIV algorithms are applied to determine the in-plane velocity components [4]–[6]. The resulting spatial resolution of the in-plane velocity field is of about 300 x 300 µm², which is less than half of the linear detector array resolution.

In comparison to state-of-the-art stereoscopic PIV systems the presented approach of combining FM-DGV and PIV to capture the entire flow field has the advantages of: only one camera and two optical accesses are needed, a higher optical robustness and an improved measurement uncertainty for the out-of-plane velocity component. Moreover, it is shown for both techniques that the high measurement rate of 10 kHz facilitates the resolution of induced sound oscillations at several kHz.

Section 2 gives an overview of the employed measurement techniques and the investigated

bias flow liner. The experimental results including a measurement uncertainty analysis are presented in section 3. Finally the paper is closed with a short summery and an outlook of future perspectives in section 4.

2. Measurement principle and setup

2.1. Approach

The FM-DGV technique is used to measure the velocity dependent Doppler shift of laser light scattered by tracer particles, which follow the flow with negligible slip. The scattered light exhibits a Doppler shifted frequency

$$f_\mathrm{D} = \frac{f_\mathrm{c}|\vec{o}-\vec{\imath}|}{c}\, v, \qquad (1)$$

where c is the speed of light, f_c the laser center frequency and v the projection of the tracer particle velocity on the sensitivity direction $\vec{o}-\vec{\imath}$ of the measurement system (cf. Fig. 1a).

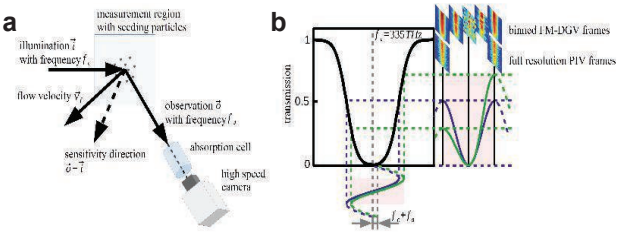

***Fig. 1: (a)** Sketch of the FM-DGV setup with resulting sensitivity direction $\vec{o}-\vec{\imath}$. **(b)** Illustration of the frequency demodulation for not Doppler shifted (purple lines) and Doppler shifted (green lines) light. For the FM-DGV evaluation a binning is applied to all recorded images for data reduction, while for the PIV evaluation only the brightest images are stored, but in full resolution.*

For the used laser wavelength of $895\ \mathrm{nm}$ the optical frequency f_c is $335\ \mathrm{THz}$. In contrast the Doppler shift f_D is merely in the MHz regime, for typical flow velocities of several $\mathrm{m\,s^{-1}}$. Therefore, a molecular absorption cell with a steep slope in the frequency dependent transmission curve is used as a frequency-intensity converter. The laser light frequency is modulated around the fine-structure transmission minimum of the cesium D1 line at $f_\mathrm{c} = 335\ \mathrm{THz}$ with

$$f_\mathrm{Laser}(t) = f_\mathrm{c} + f_\mathrm{h}\sin(2\pi f_\mathrm{m} t)\,. \qquad (2)$$

Here, f_m denotes the frequency and f_h the amplitude of the modulation signal. Due to the nonlinear transmission curve of the absorption cell the transmitted intensity signal detected with the camera contains higher-order harmonics of the modulation frequency as can be seen from Fig. 1b (green lines). The ratio

$$q(v) = \frac{A_1}{A_2} \qquad (3)$$

of the Fourier coefficients A_1 and A_2 of the first and second order harmonics depends on the measured flow velocity component v [3]. To determine the functional relationship $v = v(q)$ a calibration measurement on a rotating wheel with a known velocity is performed. In order to reduce the considerable amount of data and to shorten the evaluation time a pixel binning is applied to all measured frames.

The PIV evaluation algorithms directly determine the in-plane velocity components by an image based analysis of moving structures. Essentially, they require a high spatial resolution and strong brightness contrast [6]. Thus, the brightest images are stored in full resolution without pixel binning (cf. Fig. 1b). In addition, the PIV algorithms require an appropriate set of evaluation parameters, which is explained in the following: For a PIV evaluation the cross correlation function (CRF) between two interrogation windows is calculated by the scalar product

$$\begin{aligned} CRF &= <\phi(x,y)|T(\Delta x,\Delta y)|\psi(x,y)> \\ &= <\phi(x,y)|\psi(x+\Delta x, y+\Delta y)> \end{aligned} \qquad (4)$$

where $\phi(x,y)$ and $\psi(x,y)$ denotes the recorded intensity of the interrogation windows of subsequent images and $T(\Delta x,\Delta y)$ the translation operator. For an optimal evaluation result, first, the size of the interrogation windows has to be four times larger than the displacement of the moving structures in subsequent images. Second, the step widths Δx and Δy describing the overlap of the interrogation windows need to match the spatial offset of the moving structures [7].

As a result of the application of both evaluation techniques, FM-DGV and PIV, the entire planar velocity field can be resolved with a single camera measurement.

2.2. Setup of the measurement system

A bias flow liner, shown in Fig. 2a, is investigated to demonstrate the combination of FM-DGV and PIV for a simultaneous planar measurement of all three velocity components. The bias flow of about $7\ \mathrm{m\,s^{-1}}$ is regulated by a mass flow controller and fed with seeding particles provided by a commercial particle generator. The seeding particles are made of diethylhexyl sebacate (DEHS) and have a particle diameter of about $1\ \mu\mathrm{m}$. The suction is realized by a duct fan where the suction flow is directed in the negative x-direction (cf. Fig. 2a). The measurements are performed at the central of 53 orifices (each with a diameter of $2.5\ \mathrm{mm}$) marked by the blue rectangle in Fig. 2a. To study the damping phenomena a sinusoidal acoustic excitation signal at $f_\mathrm{ac} = 867\ \mathrm{Hz}$ with a sound pressure level of $120\ \mathrm{dB}$ is applied by a speaker of the type KU-516 from the manufacturer MONACOR. In addition, the total harmonic distortion is estimated using a reference microphone to 0.8%. The measurement region provides an optical access

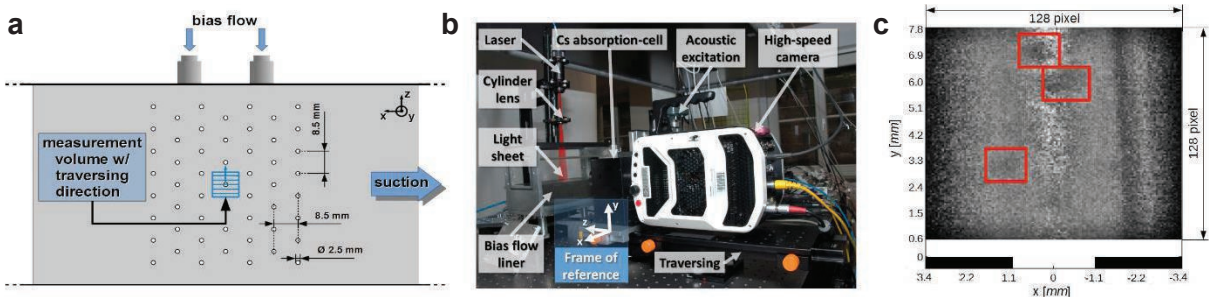

Fig. 2: ***(a)*** *Measurements at the central orifice (blue rectangle) of a perforated liner with bias flow were performed.* ***(b)*** *The test rig is acoustically excited by a speaker and the sound-flow interaction is measured using the FM-DGV system in combination with a high-speed camera.* ***(c)*** *Full resolution image of 128 x 128 pixel at z = 0 (equals the center of the orifice) with enhanced contrast. The red rectangles mark the characteristic flow structures.*

through three glass windows. A laser light sheet illuminates the x-y-plane and the light scattered at seeding particles is measured with a high-speed camera mounted behind the cesium absorption cell as shown in Fig. 2b. Additionally, an aperture diaphragm is used to avoid the detection of light reflections from the liner surface. This facilitates the measurement of near-field phenomena merely $600\ \mu\mathrm{m}$ above the central orifice. The 3D velocity field is finally obtained by traversing the light sheet together with the camera along the z-direction in 8 steps of $450\ \mu\mathrm{m}$ over $3.6\ \mathrm{mm}$.

The camera operates at a frame rate of 100 kHz with a resolution of 128 x 128 pixel, giving a maximum continuous duration of $18.5\ \mathrm{s}$ (i.e. 1.9 million frames) per acquisition. For averaging, five repeated acquisitions are recorded and evaluated for each z-position. Due to the lens system attached to the cesium absorption cell with a magnification ratio of two the observed region spans approximately 7.2 x 7.2 mm² in the x-y-pane (pixel size 28 x 28 µm²).

In principle, the FM-DGV technique combined with a camera allows a high spatial resolution up to a single pixel. Hence, the minimal resolution in x- and y-direction amounts to 56 x 56 µm². However, a binning of 4 x 4 pixel is applied improving the uncertainty and decreasing the amount of data to be processed. The resolution in z-direction is limited by the light sheet thickness and is approximately 300 µm. The resulting spatial resolution of 220 x 220 x 300 µm³ is sufficient, because it is about one order of magnitude smaller than the orifice diameter in its dimension. As a result, the 3D FM-DGV data consists of 32 x 32 x 9 voxels. The laser is modulated with $f_\mathrm{m} = 10\ \mathrm{kHz}$, which is the maximum measurement rate for FM-DGV at this camera configuration. Consequently, sound induced flow oscillations can be resolved up to $5\ \mathrm{kHz}$ according to the Nyquist-Shannon sampling theorem.

Since a comparison between FM-DGV and PIV regarding the measurement uncertainty and spectral resolution is intended, two FM-DGV measurements are required to obtain the velocity components in the y- and z-direction. The FM-DGV measurements are performed successively from different observation directions. This allows a validation of velocity component in y-direction by comparing the results of the PIV and FM-DGV evaluation. As can be seen from Fig. 2b the first measurement is performed from the observation direction $\vec{o}_1 = (0,0,-1)$. The second measurement (not shown here) is done from the opposite liner site with $\vec{o}_2 = (0,0,+1)$. During these measurements the illumination direction $\vec{\imath} = (0,-1,0)$ is not changed. Since the resulting sensitivity directions are perpendicular to each other, the coordinate transformation of the measured velocity components v_1 and v_2 is given by

$$\begin{pmatrix} v_x \\ v_y \end{pmatrix} = \begin{pmatrix} \cos\varphi & -\sin\varphi \\ \sin\varphi & \cos\varphi \end{pmatrix} \begin{pmatrix} v_1 \\ v_2 \end{pmatrix} \quad (5)$$

where $\varphi = -45°$ denotes the rotation angle and v_x and v_y the velocity components of the reference frame (cf. Fig. 2a).

The PIV evaluation of the full resolution images spanning 128 x 128 pixel uses the open source software PivLab. The high seeding concentration prohibits a resolution of single particles as can be seen from Fig. 2c. However, since the PIV algorithms calculate the CRF of shifted interrogation windows it is merely needed to resolve moving structures (in contrast to particle tracking algorithms). As can be seen from Fig. 2c the maximum size of these structures is about 25 x 25 pixel. The displacement of moving structures in subsequent images can be estimated from the expected bias flow of $7\ \mathrm{m\,s^{-1}}$ and the PIV image acquisition rate of $20\ \mathrm{kHz}$, and amounts to approximately $6\ \mathrm{pixel}$. The interrogation window size of the first pass of the evaluation routine is chosen four times larger than the displacement to 24 x 24 pixel to avoid erroneous correlations and minimize the measurement uncertainty [7]. Since this means a strong reduction of the number of measurement points of the velocity field to merely 5 x 5, a second pass with 12 x 12 pixel and a third pass with 6 x 6 pixel is

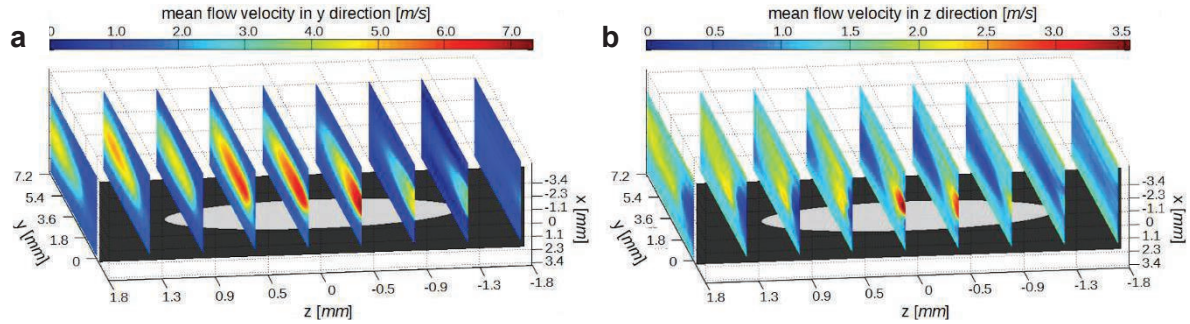

Fig. 3: (a) *The mean flow velocity in y-direction with a maximal value of 7.2 m s^{-1}.* ***(b)*** *The mean flow velocity in z-direction with a maximal value of 3.5 m s^{-1}.*

processed. The interrogation window overlap is in all cases adjusted to 50%, which equals a step width of 12 pixel in the first, of 6 pixel in the second and of 3 pixel in the third pass of the evaluation routine. This finally results in a spatial resolution of 280 x 280 x 300 µm³ consisting of a dataset of 24 x 24 x 9 voxels for the both velocity components in x- and y-direction. Due to the symmetric modulation around the center frequency of the non-linear transmission curve the intensity signal is dominated by the second harmonic. As a consequence, two bright images per modulation can be used for the PIV evaluation. Thus, the image recording rate amounts to $20\ \mathrm{kHz}$. Since two subsequent images give one flow velocity field the PIV measurement rate halves to $10\ \mathrm{kHz}$, which is in accordance with the FM-DGV acquisition rate. This simplifies the combination of both techniques.

3. Results

3.1. FM-DGV evaluation

Fig. 3 shows the mean flow velocities measured with FM-DGV. For a better visibility the orifice is stretched along the z-direction. Since the velocity component in x-direction can be neglected (the PIV evaluation revealed a maximal mean flow of $0.4\ \mathrm{ms}^{-1}$) the maximum flow velocity amounts to the absolute value of the vectorial addition of the maximal velocity of $7.2\ \mathrm{ms}^{-1}$ in y-direction and of $3.5\ \mathrm{ms}^{-1}$ in z-direction, which yields $8.0\ \mathrm{ms}^{-1}$. The magnitude of this resulting velocity vector is in good agreement with the estimated value of $7\ \mathrm{ms}^{-1}$ calculated from the controlled mass flow. Due to the suction flow the mean flow is slight tilted towards the negative x-direction (cf. Fig. 3a and Fig. 3b). Furthermore, the flow leaves the orifice slightly oblique in z-direction, which is attributed to the asymmetric feeding of the bias flow only from the positive z-direction (see Fig. 2a).

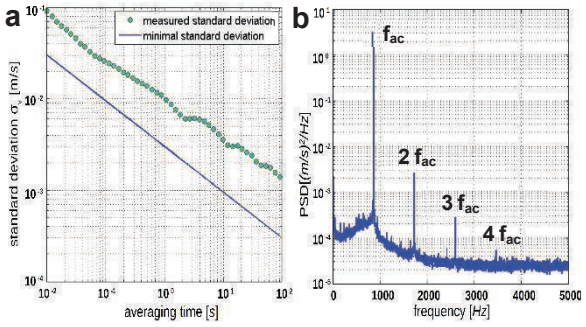

Fig. 4: (a) *The measured standard deviation reduces with the averaging time, but is about one order of magnitude larger than the minimal reachable standard deviation in case without turbulences* [10]. ***(b)*** *The power spectral density (PSD) at x = 0, y = 2.3 mm and z = 0 for the velocity component in y-direction reveals characteristic peaks at the acoustic excitation frequency f_{ac} = 867 Hz and its higher harmonics.*

In Fig. 4a the standard deviation of the mean velocity in y-direction (green points) is shown as an example for x = 0, y = 2.3 mm and z = 0 for different averaging times. The temporal averaging over 90 s leads to a theoretical uncertainty limit of $0.3\ \mathrm{mms}^{-1}$ [8]. However, the measured velocity uncertainty of $1.4\ \mathrm{mms}^{-1}$ is one order of magnitude larger than the theoretical uncertainty limit due to flow turbulence. In addition, Fig. 4b exhibits the one-sided power spectral density (PSD) at x = 0, y = 2.3 mm and z = 0. Besides the characteristic peak at the acoustic excitation frequency of $f_{\mathrm{ac}} = 867\ \mathrm{Hz}$ higher order harmonics are measured. Calculating the total harmonic distortion from the PSD gives 3%, which is larger than the harmonic distortion of the speaker system of 0.8% (cf. section 2.2). This indicates a non-linear behavior of the bias flow liner. Since former publications reveal a correlation between the excitation of higher harmonics and the damping efficiency it is assumed that this nonlinearities are an essential factor for sound-flow interactions [9]. Furthermore, the PSD decreases with increasing frequency, which is typical for turbulence spectra. These turbulences explain the difference between the theoretical and the measured standard deviation. Moreover, Fig. 5 presents the amplitudes of the sound induced oscillation velocity based on the Fourier coefficients of the time series at $f_{\mathrm{ac}} = 867\ \mathrm{Hz}$ for both velocity components. In coincidence with the mean flow velocity field, regions with a large amplitude exhibit an increasing liftoff from the liner surface in positive z-direction. Moreover, sound induced oscillations are excited in the vicinity of the orifice

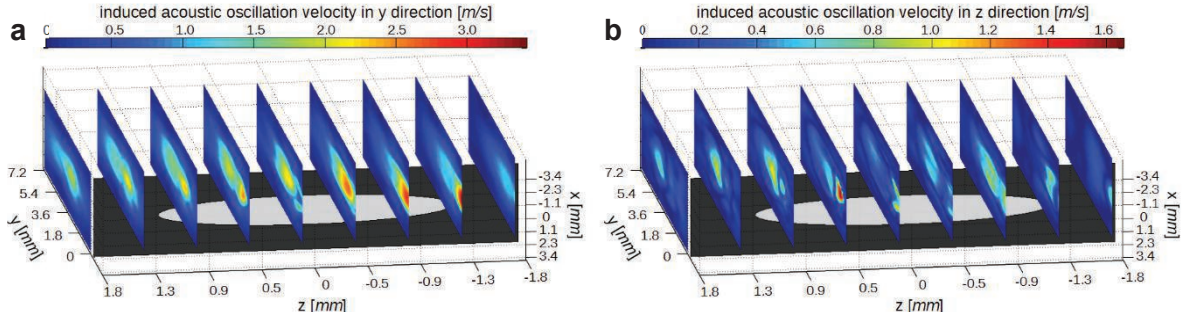

Fig. 5: (a) *The amplitudes of the acoustically induced flow oscillation velocity in y-direction at f_{ac} = 867 Hz.* ***(b)*** *The amplitudes of the acoustically induced flow oscillation velocity in z-direction at f_{ac} = 867 Hz.*

periphery, which are regions with a high vorticity. Thus, two factors seems responsible for an enhanced energy transfer from the sound into flow: a high mean flow velocity and a high vorticity.

The dataset further allows a phase-resolved analysis of the flow oscillation as shown in Fig. 6a for the measurement plane at z = 0.5 mm. As a result, two maxima occur, whose distance of 0.4 cm is two orders of magnitude smaller than the acoustic wavelength of 38 cm. This implies the generation of vortices fluctuating with the acoustic excitation frequency. According to the time evolution during one acoustic period in Fig. 6a the vortices detach from the liner surface and decompose at 5.4 mm above the orifice. This dissipative energy transfer, i.e. the excitation of vortices, their decomposition and the transfer into heat is the reason for the high damping performance. Moreover, Fig. 6b presents the time evolution over one period at x = 0, y = 2.4 mm and z = 0.5 mm. The velocity fluctuation is dominated by the first order harmonic since it is at least three orders of magnitude larger than the magnitude of higher orders (cf. Fig. 4b). As a result the velocity fluctuates almost sinusoidal between $0\,\mathrm{ms}^{-1}$ and $4\,\mathrm{ms}^{-1}$ within one period.

3.2. Combination with PIV

In order to extract all three velocity components from a single measurement PIV algorithms are additionally applied to determine the in-plane velocity components. This allows a simultaneous

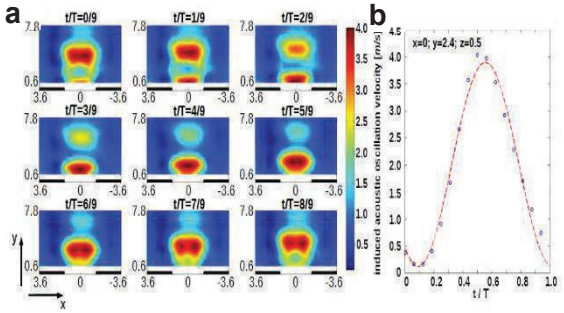

Fig. 6: (a) *The phase-resolved oscillations at z = 0.5 mm over one period of T = 1/(867 Hz).* ***(b)*** *The time evolution of the oscillations at x = 0, y = 2.4 mm and z = 0.5 mm exhibit a predominantly sinusoidal character.*

measurement of the entire velocity field with a high spatial and temporal resolution using a single camera and, thus, facilitates the investigation of unsteady flow phenomena. As an example only the measurement plane at z = 0 is considered here. Fig. 7 presents a comparison of the mean flow velocity in y-direction obtained from

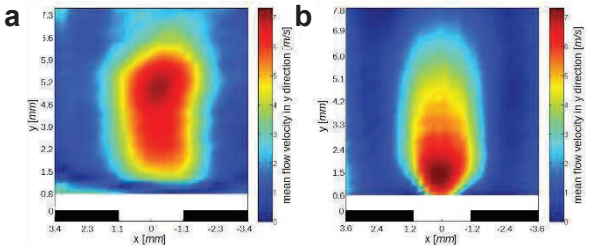

Fig. 7: (a) *The mean flow velocity in y-direction at z = 0 taken from the PIV evaluation exhibits the maximal flow velocity at 4.7 mm above the center of the orifice.* ***(b)*** *The mean flow velocity in y-direction at z = 0 taken from the FM-DGV evaluation exhibits the maximal flow velocity at 1.3 mm above the center of the orifice.*

the FM-DGV measurement (right) and that of the PIV evaluation (left). The results differ in their shape and positioning relative to the orifice. However, the maximum flow velocities of $7.1\,\mathrm{ms}^{-1}$ for the FM-DGV and of $7.0\,\mathrm{ms}^{-1}$ for the PIV evaluation are in good agreement. It is known that PIV algorithms fail especially in regions with a high out-of-plane velocity component [7]. According to the maximal velocity of $3.5\,\mathrm{ms}^{-1}$ in z-direction, a light sheet thickness of

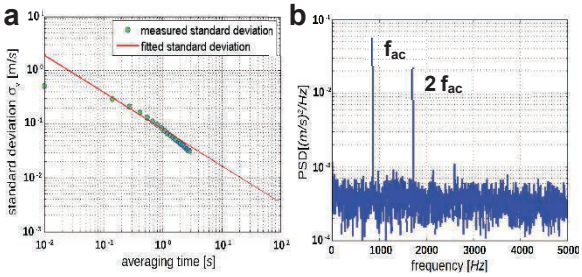

Fig. 8: (a) *The measured standard deviation reduces with the square root of the averaging time.* ***(b)*** *The power spectral density (PSD) at x = 0, y = 2.3 mm and z = 0 for the velocity component in y-direction reveals characteristic peaks at the acoustic excitation frequency f_{ac} = 867 Hz and its second harmonic of 1734 Hz.*

$300\ \mu m$ and an image acquisition rate of $20\ kHz$, a particle crosses the light sheet within two acquisitions. This is responsible for a strong intensity fluctuation and prohibits a successful PIV evaluation near the orifice. To encounter this problem the light sheet thickness should be increased in future setups.

In accordance to the FM-DGV results, Fig. 8 presents the standard deviation for different averaging times and the PSD at the same position for the PIV evaluation of the mean flow velocity component in y-direction. An averaging over 2.5 s leads to a standard deviation of $20\ mm s^{-1}$. Extrapolating the measurement uncertainty for an averaging time of 90 s, as used for FM-DGV, reveals $4\ mm s^{-1}$ (cf. Fig. 8a red line). This is almost three times larger than the FM-DGV velocity uncertainty.

Moreover, the spectral analysis shown in Fig. 8b exhibits a peak at the acoustic exciation frequency of $f_{ac} = 867\ Hz$. Thus, an evaluation of the acoustically induced oscilation velocity at $f_{ac} = 867\ Hz$ seems resonable. A comparison of the FM-DGV and the PIV evaluation is shown in Fig. 9.

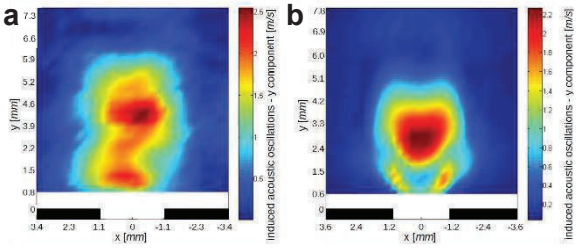

***Fig. 9: (a)** The acoustically induced oscillation velocity at z = 0 extracted from the PIV evaluation at f_{ac} = 867 Hz. **(b)** The acoustically induced oscillation velocity at z = 0 extracted from the FM-DGV data at f_{ac} = 867 Hz.*

Both techniques deliver nearly the same maximal oscillation amplitudes (FM-DGV: $2.2\ ms^{-1}$, PIV: $2.5\ ms^{-1}$), but the measured spatial distributions of the velocity oscillations differ. Especially the PIV results appear to be blurred. Possible reasons for this difference are the reduced are the reduced resolution of 24 x 24 pixel and the currently lower averaging time for the PIV evaluation. Furthermore, the mentioned variation of the particle presence in the light sheet plane might contribute, which has to be investigated further. However, the principle phenomena of an increased oscillation above the liner orifice is in agreement with the FM-DGV results.

4. Summary and Outlook

The applicability of a high-speed camera in combination with a FM-DGV system is successfully proven on a liner test rig. Due to the high measurement rate the spectrum is resolved up to $5\ kHz$, which enables e.g. the analysis of higher order harmonics and turbulences. In addition to the mean flow velocity, sound induced oscillations of several kHz are resolved. This is a key demand for a better understanding of the occurring acoustic damping effects and an improvement of the damping performance. Furthermore, the measurements exhibit a noteworthy spatial resolution of 220 x 220 x300 µm³ for the FM-DGV system.

The performed PIV evaluation is in accordance with the FM-DGV results. Even acoustically induced oscillations could be resolved up to $5\ kHz$, which is validated by the FM-DGV measurements. The achieved spatial resolution of amounts to 280 x 280 x 300 µm³. A further improvement and analysis of the limiting factors promises a measurement technique, which is capable to record the entire planar flow field with a single camera measurement, simultaneously.

Acknowledgement

The authors thank the German Research Foundation (DFG) for funding the projects CZ 55/25-1 and EN 797/2-1. Many thanks go to Jörg König for the helpful discussions.

References

[1] J. D. Eldredge, A. P. Dowling, The absorption of axial acoustic waves by a perforated liner with bias flow, *J. Fluid Mech.* 485, 307–335 (2003); doi: 10.1017/s00221-12003004518

[2] D. Haufe et al., Optical multi-point measurement of the acoustic particle velocity in a superposed flow using a spectroscopic laser technique, *Meas. Sci. Technol.* 23 (2012); doi: 10.1088/0957-0233/23/8/085306

[3] A. Fischer et al., Investigation of time-resolved single detector Doppler global velocimetry using sinusoidal laser frequency modulation, *Meas. Sci. Technol.* 18, 2529–2545 (2007), doi: 10.1088/0957-0233/18/8/029

[4] R. Boemmels, T. Roesgen, Development of a planar three-component velocimeter using Doppler global velocimetry (DGV) and PIV, *19th International Congress on Instrumentation in Aerospace Simulation Facilities*, 211–218 (1991)

[5] M. P. Wernet, Planar particle imaging Doppler velocimetry: a hybrid PIV/DGV technique for three-component velocity measurements, *Meas. Sci. Technol.* 15, 2011–2028 (2004); doi: 10.1088/0957-0233/15/10/011

[6] C. Willert et al., Combined PIV and DGV applied to a pressurized gas turbine combustion facility, *Meas. Sci. Technol.* (17), 1670–1679 (2006); doi: 10.1088/0957-0233/17/7/005

[7] R. D. Keane, R. J. Adrian, Optimization of particle image velocimeters, *Meas. Sci. Technol.* (1), 1202–1215 (1990); doi: 10.1088/0957-0233/1/11/013

[8] A. Fischer et al., Optical multi-point measurements of the acoustic particle velocity with frequency modulated Doppler global velocimetry, *J. Acoust. Soc. Am.* (134), 1102–11 (2013); doi: 10.1121/1.4812753

[9] D. Haufe et al., Spectral analysis of the flow sound interaction at a bias flow liner, *Appl. Acoust.* (81), 47–49 (2014); doi: 10.1016/j.apacoust.2014.02.007

[10] D. Haufe et al., Multi-scale measurement of acoustic particle velocity and flow velocity for liner investigations, *Exp. Fluids* (54), 1569 (2013); doi: 10.1007/s00348-013-1569-4